Supporting Information

Synergistic color-changing and conductive photonic cellulose nanocrystal patches for sweat sensing with biodegradability and biocompatibility

Yi Qian,[a] Hao Wang,[a] Zhen Qu,[a] Qiongya Li,[b] Dongdong Wang,[b] Xindi Yang,[b] Haijuan Qin,[c] Haijie Wei,[b] Fusheng Zhang*[ab] and Guangyan Qing*[ab]

[a] Hubei Key Laboratory of Biomass Fibers and Eco-dyeing & Finishing, College of Chemistry and Chemical Engineering, Wuhan Textile University, Wuhan 430200 P. R. China
[b] CAS Key Laboratory of Separation Science for Analytical Chemistry, Dalian Institute of Chemical Physics, Chinese Academy of Sciences, Dalian 116023, P. R. China
[c] Research Centre of Modern Analytical Technology, Tianjin University of Science and Technology, Tianjin 300000, P. R. China

E-mail: fszhang@wtu.edu.cn, qinggy@dicp.ac.cn

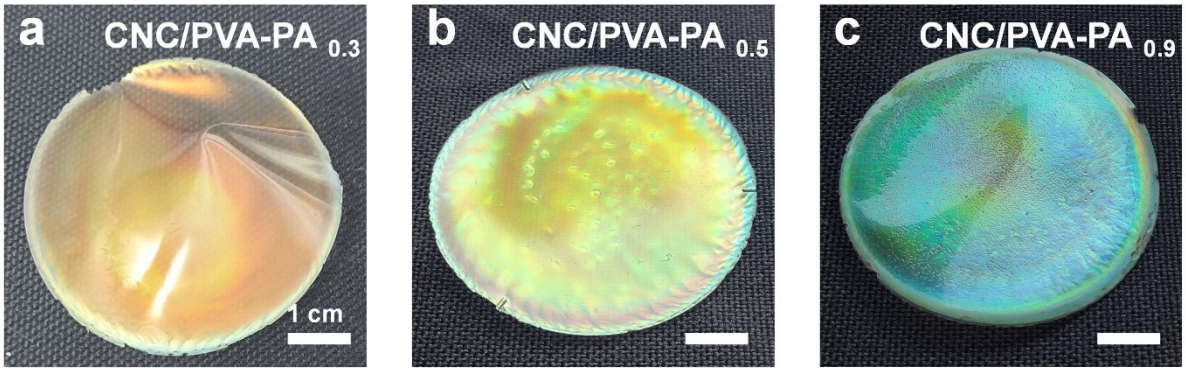

Figure S1. Photographs of CNC/PVA-PA films treatment with 30 wt% (a), 50 wt% (b), and 90 wt% (c) PA solution.

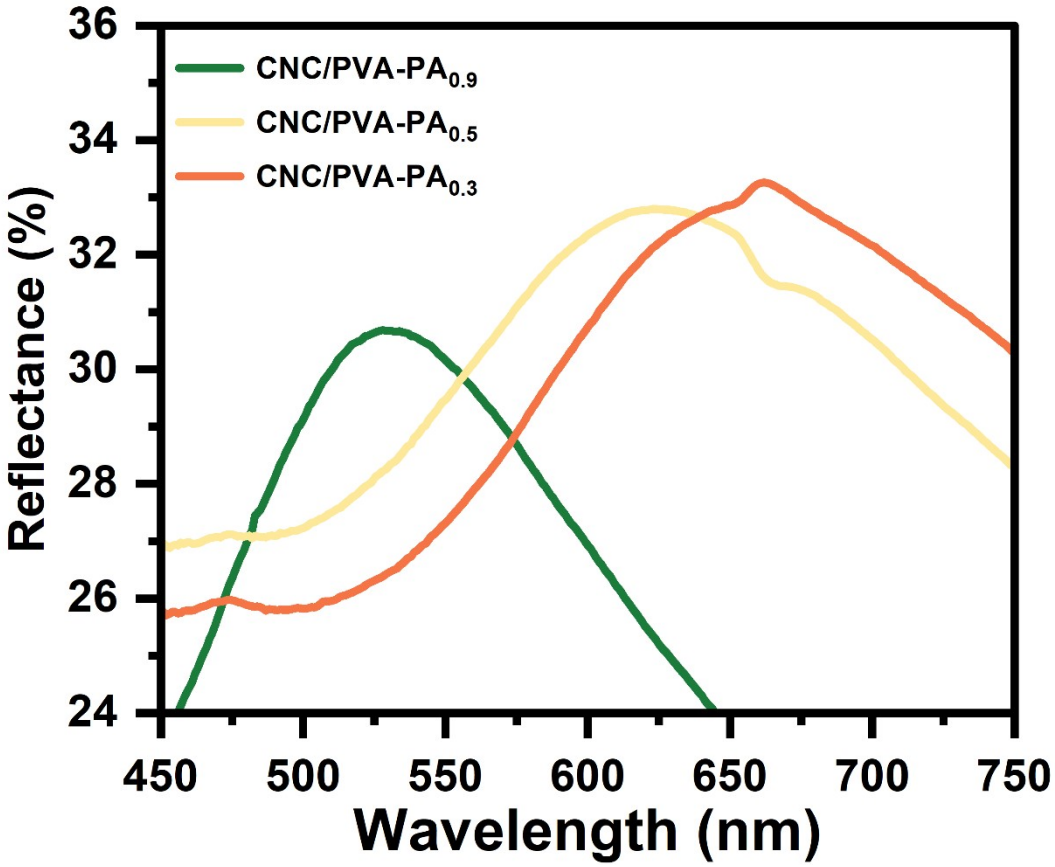

Figure S2. UV–vis reflectance spectra of CNC/PVA-PA films treatment with 30 wt% (a), 50 wt% (b), and 90 wt% (c) PA solution.

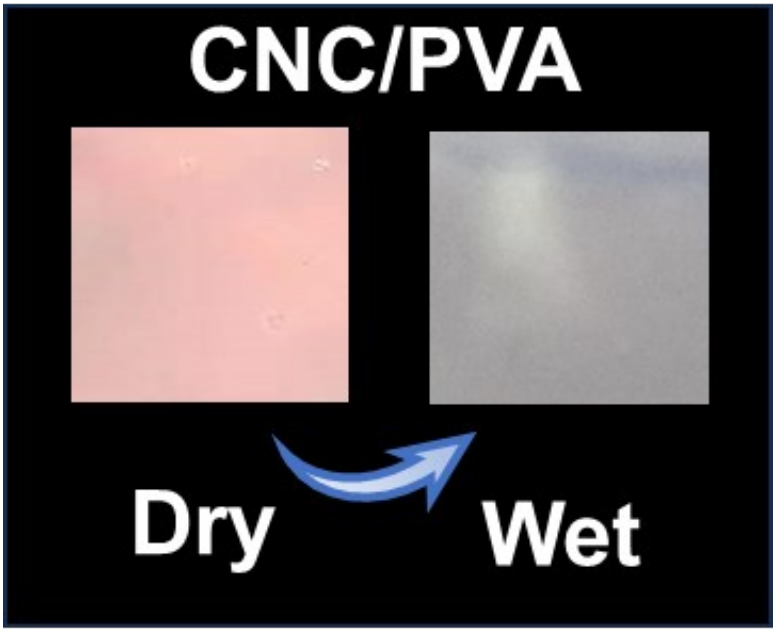

Figure S3. Photographs of CNC/PVA film before and after wet with water.

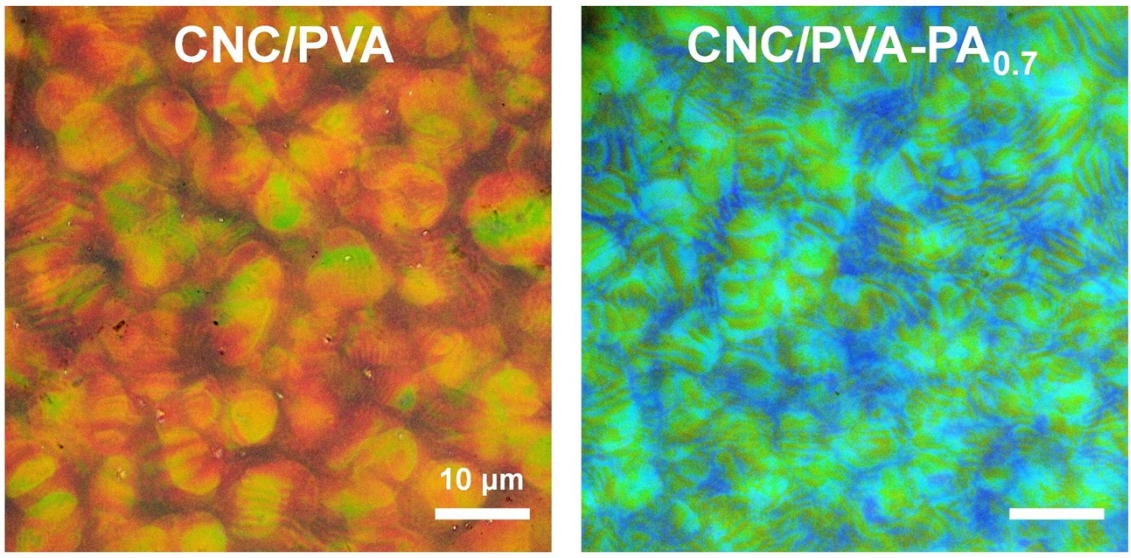

Figure S4. POM images of CNC/PVA and CNC/PVA-$PA_{0.7}$ films.

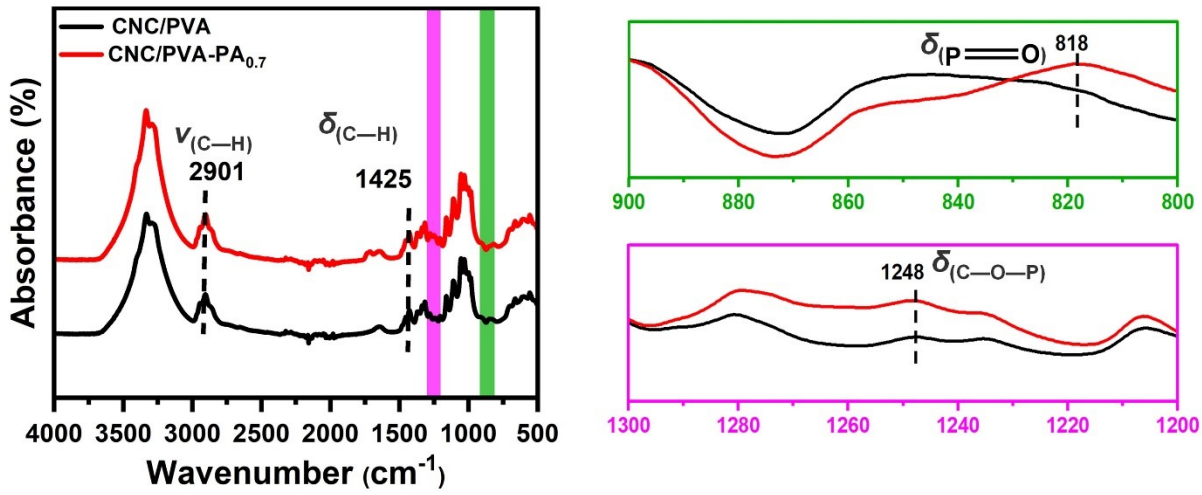

Figure S5. ATR–FTIR spectra of CNC/PVA and CNC/PVA-$PA_{0.7}$ films.

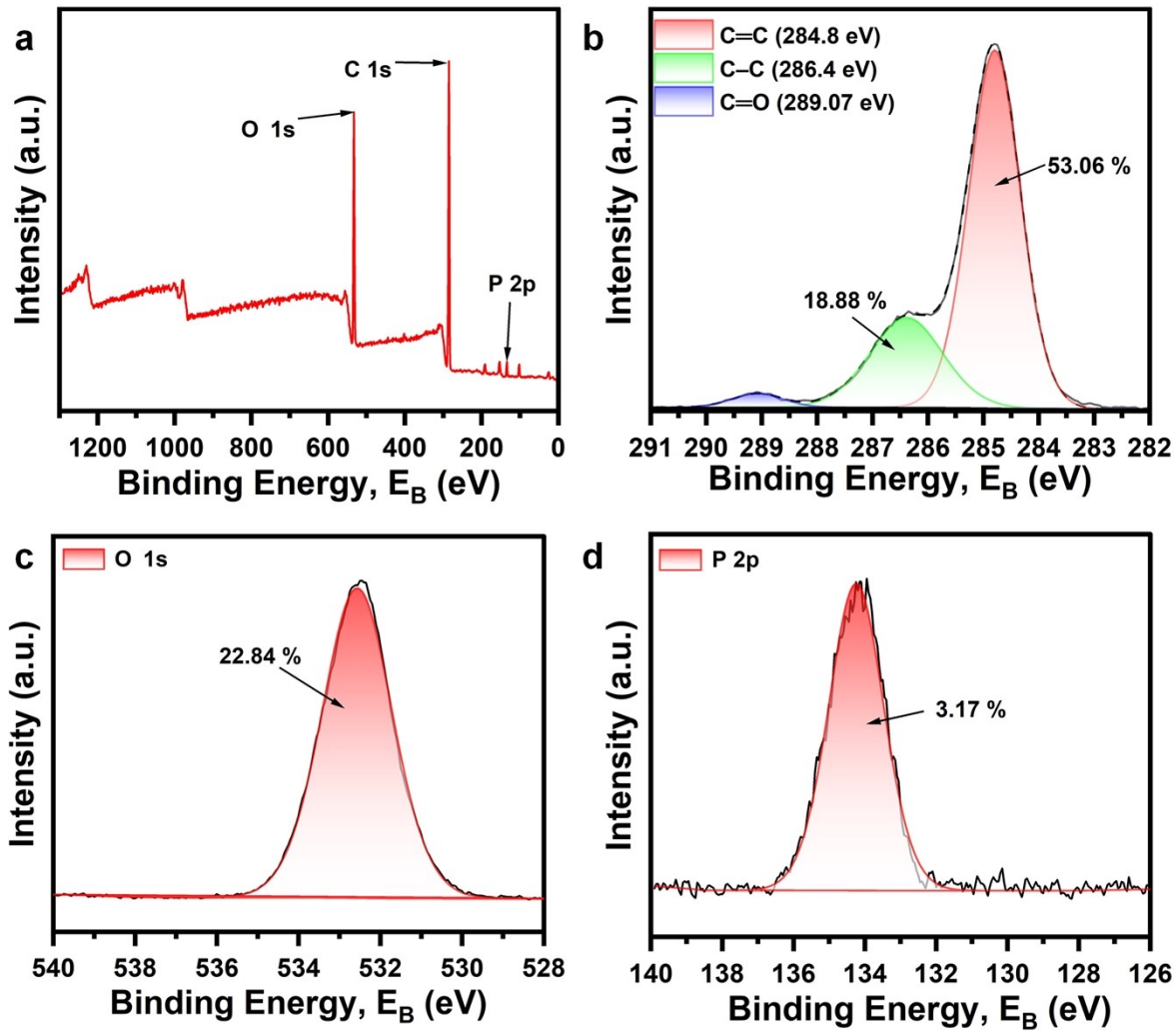

Figure S6. The overall XPS spectra(a), C 1s region (b), O 1s region (c), and P 2p region (d) of CNC/PVA-$PA_{0.7}$ films.

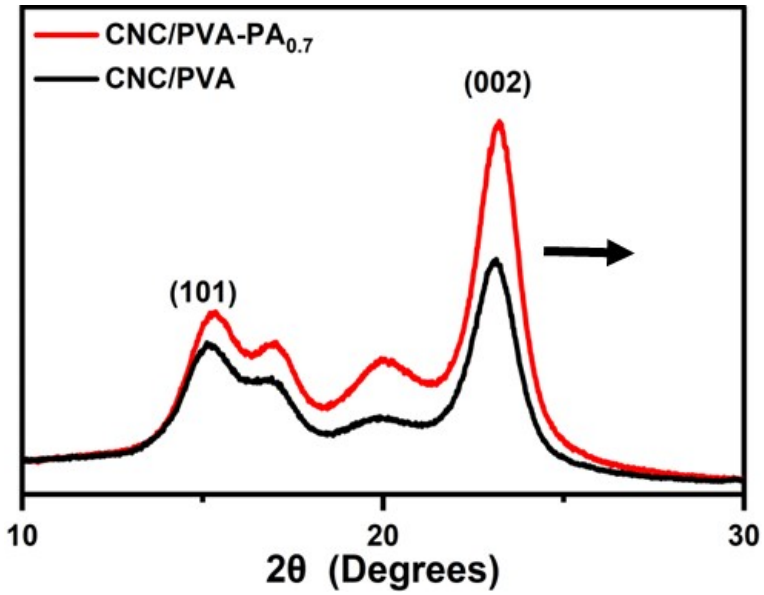

Figure S7. XRD patterns of CNC/PVA and CNC/PVA-$PA_{0.7}$ films.

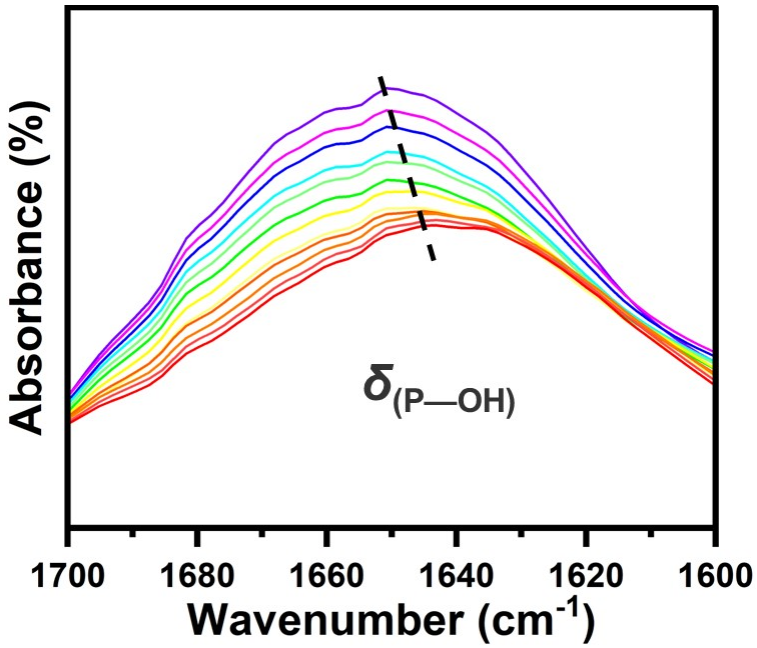

Figure S8. Amplified in situ FTIR spectra of CNC/PVA-$PA_{0.7}$ films treated from 20 to 60 °C.

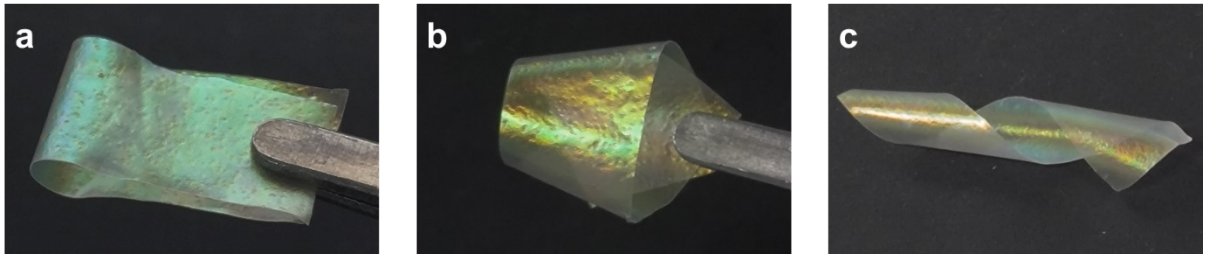

Figure S9. Photographs of CNC/PVA-$PA_{0.7}$ films after bending (a), folding(b), and twisting (c).

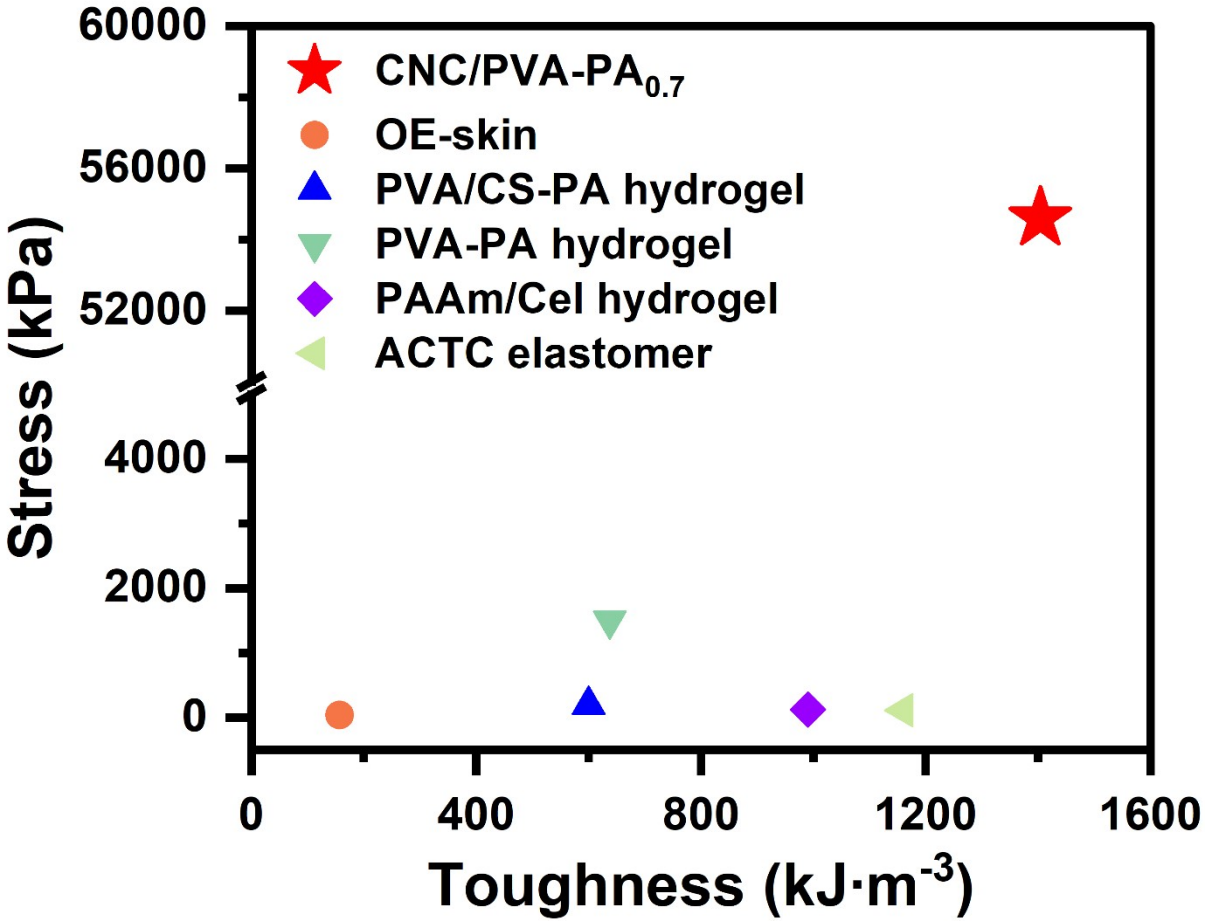

Figure S10. Comparison of stress and toughness values with similar materials reported in the literature.[1–5]

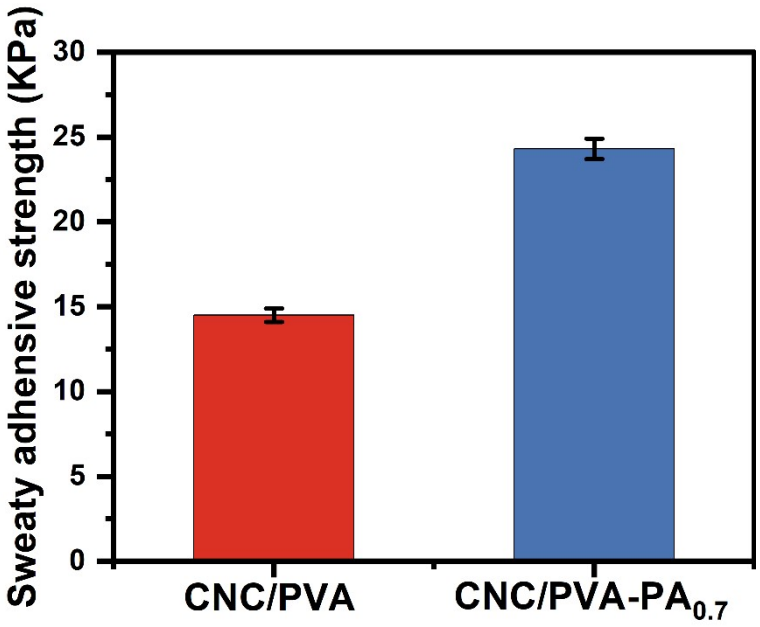

Figure S11. The adhesive strength of the CNC/PVA and CNC/PVA-$PA_{0.7}$ films after pressing on pig skins that wetted by 10 μL sweat.

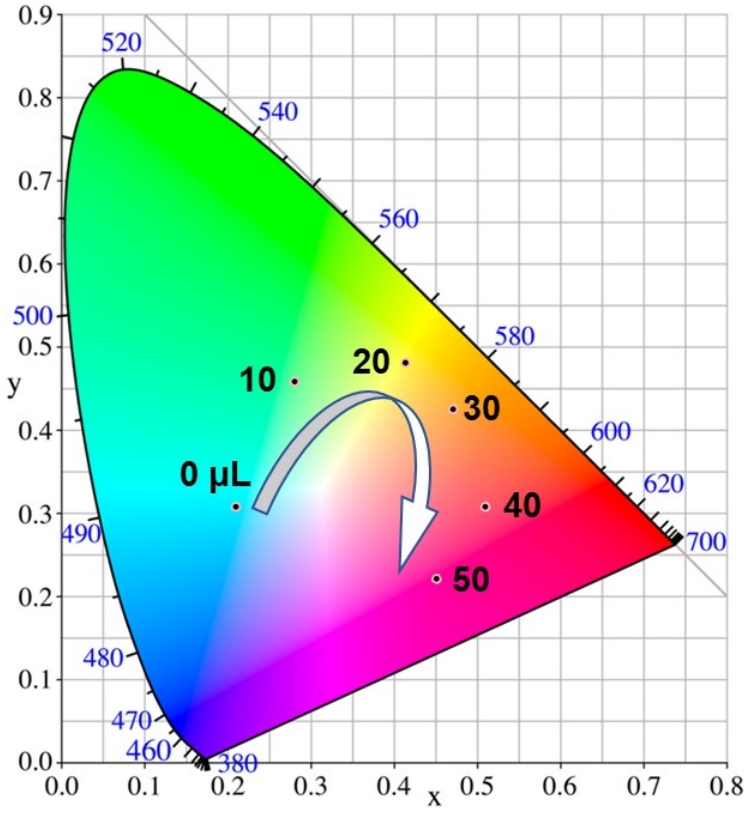

Figure S12. CIE chromaticity diagram versus different sweat volumes.

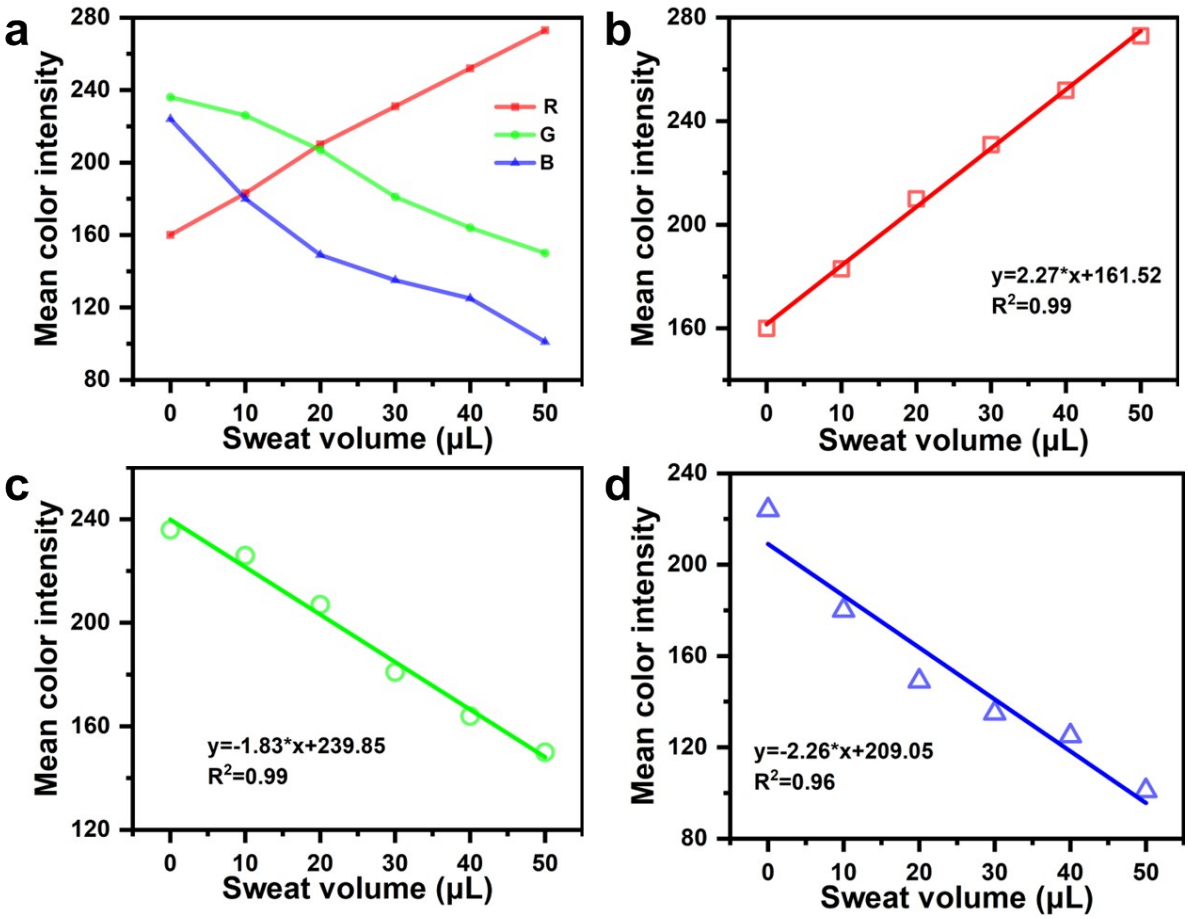

Figure S13. RGB changes of colorimetric detection units during the detection of sweat volumes.

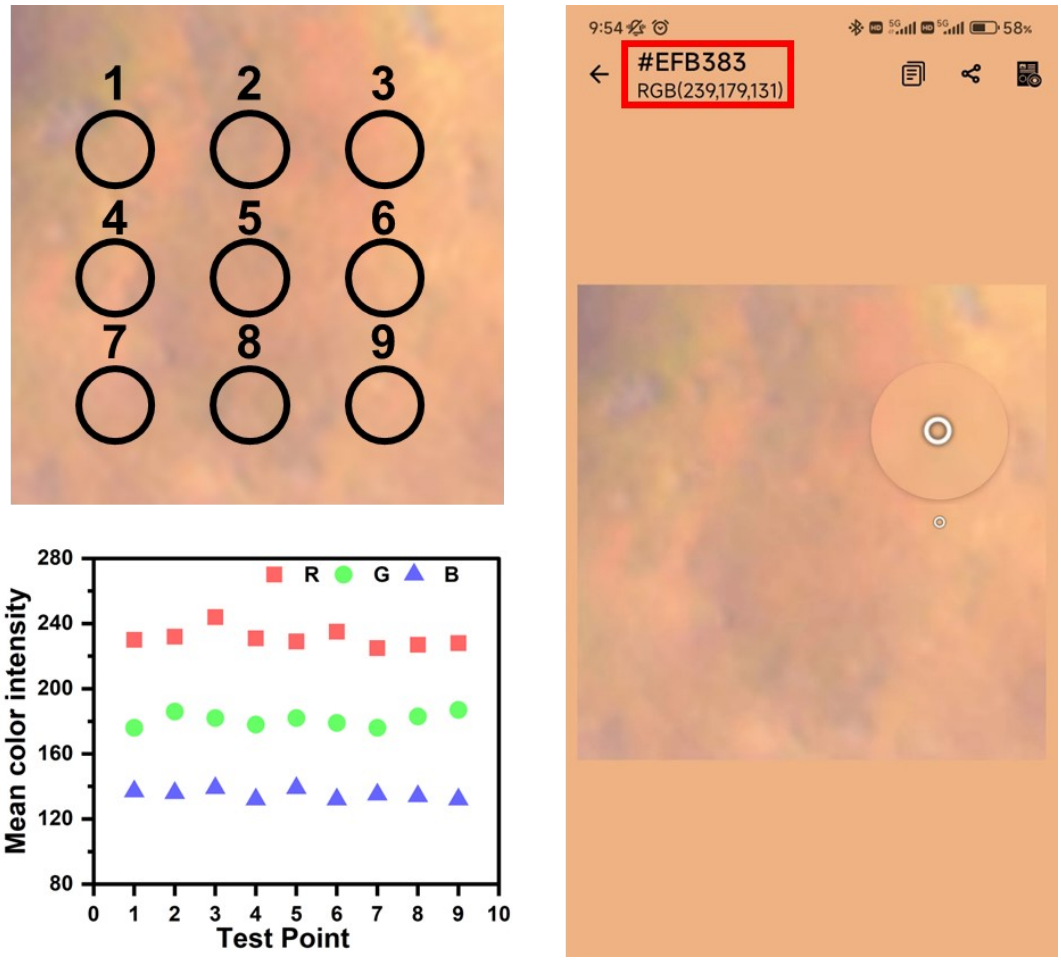

Figure S14. Image of RGB analysis about nine points at different positions based on a smartphone application.

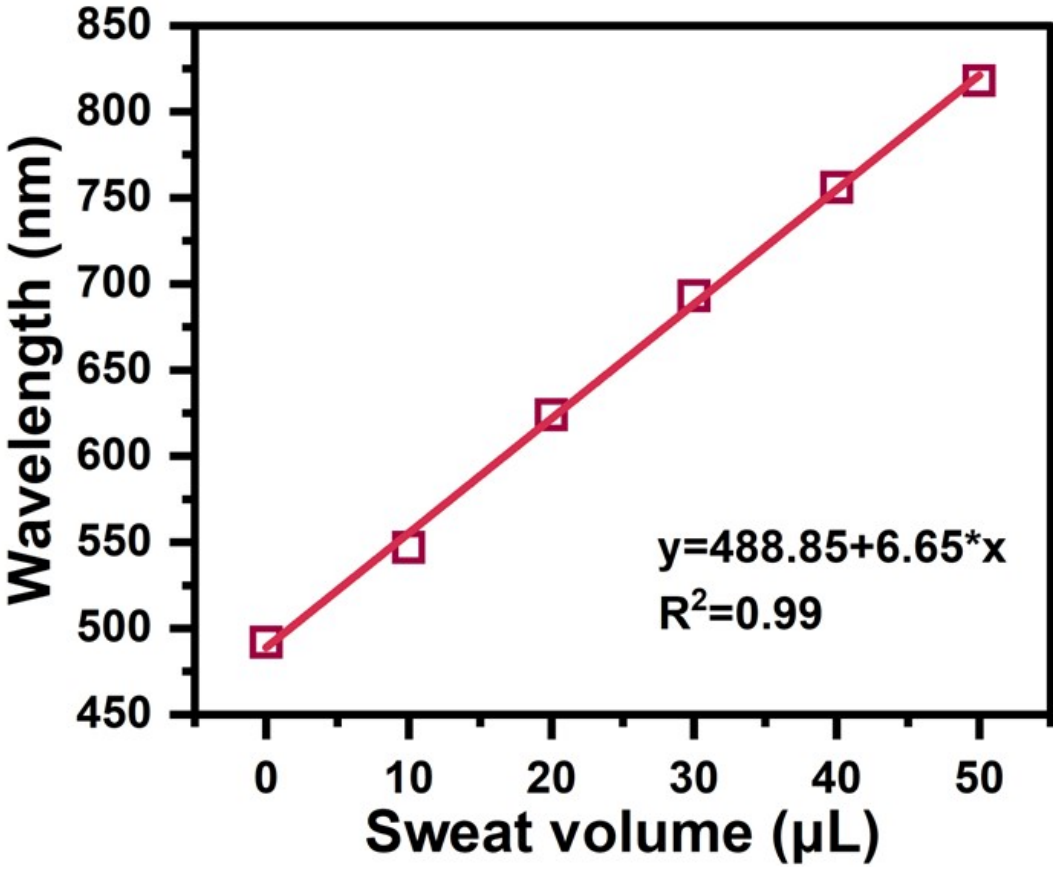

Figure S15. Wavelength of the OEDS patch versus different sweat volumes.

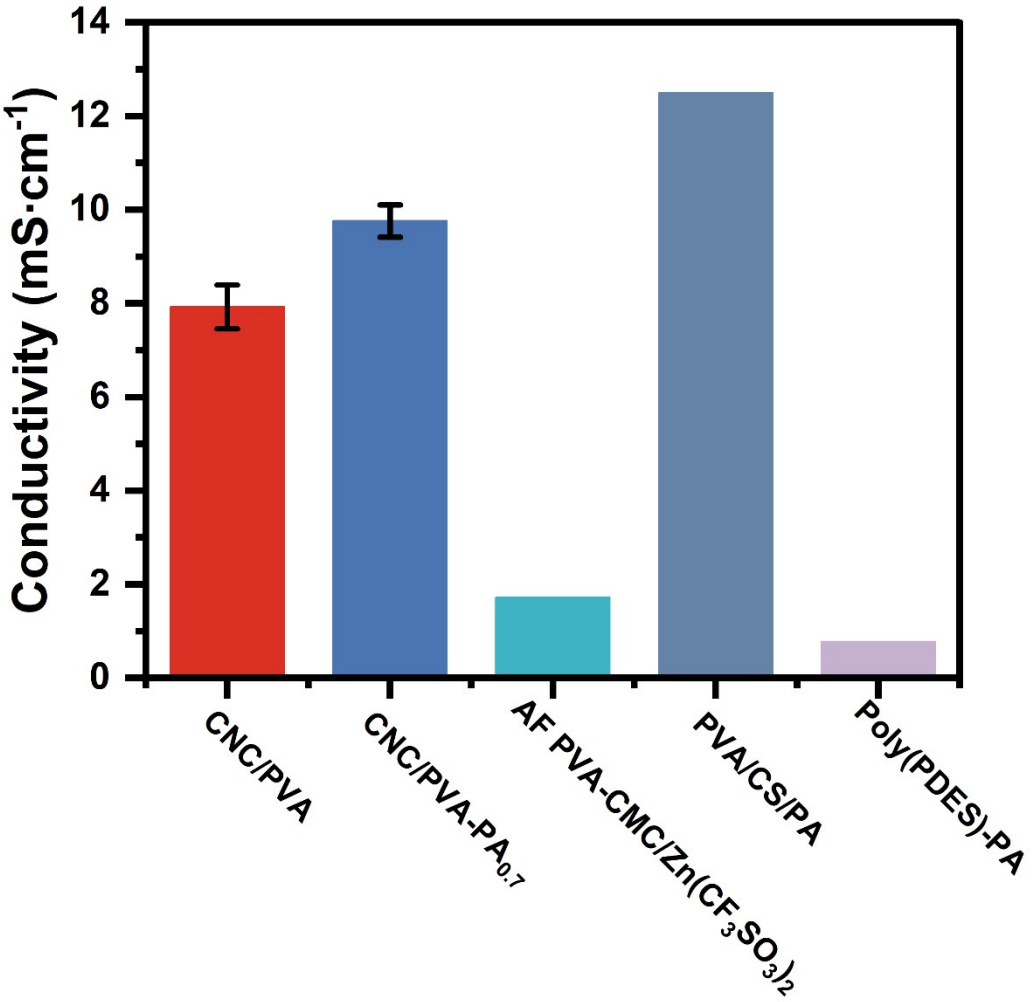

Figure S16. The conductivity of CNC/PVA, CNC/PVA-$PA_{0.7}$, and other similar.[1,6,7]

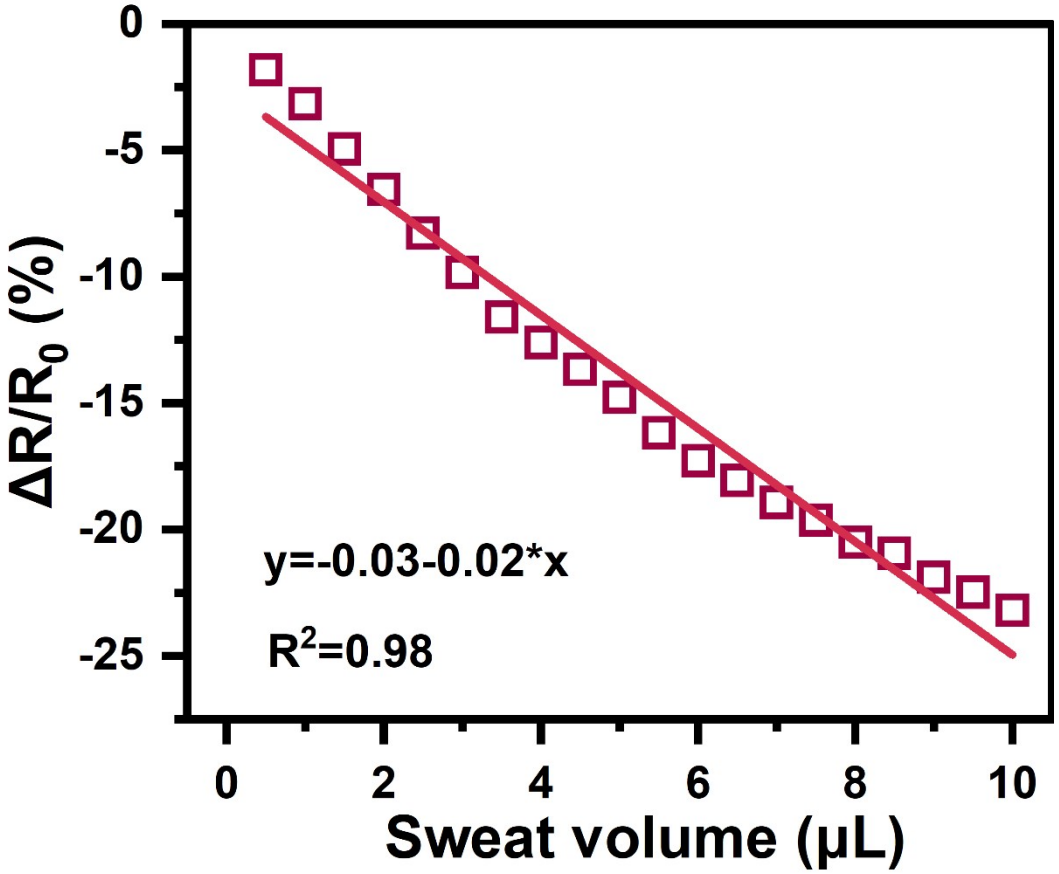

Figure S17. Correlation of resistivity and sweat volume of CNC/PVA-$PA_{0.7}$ films.

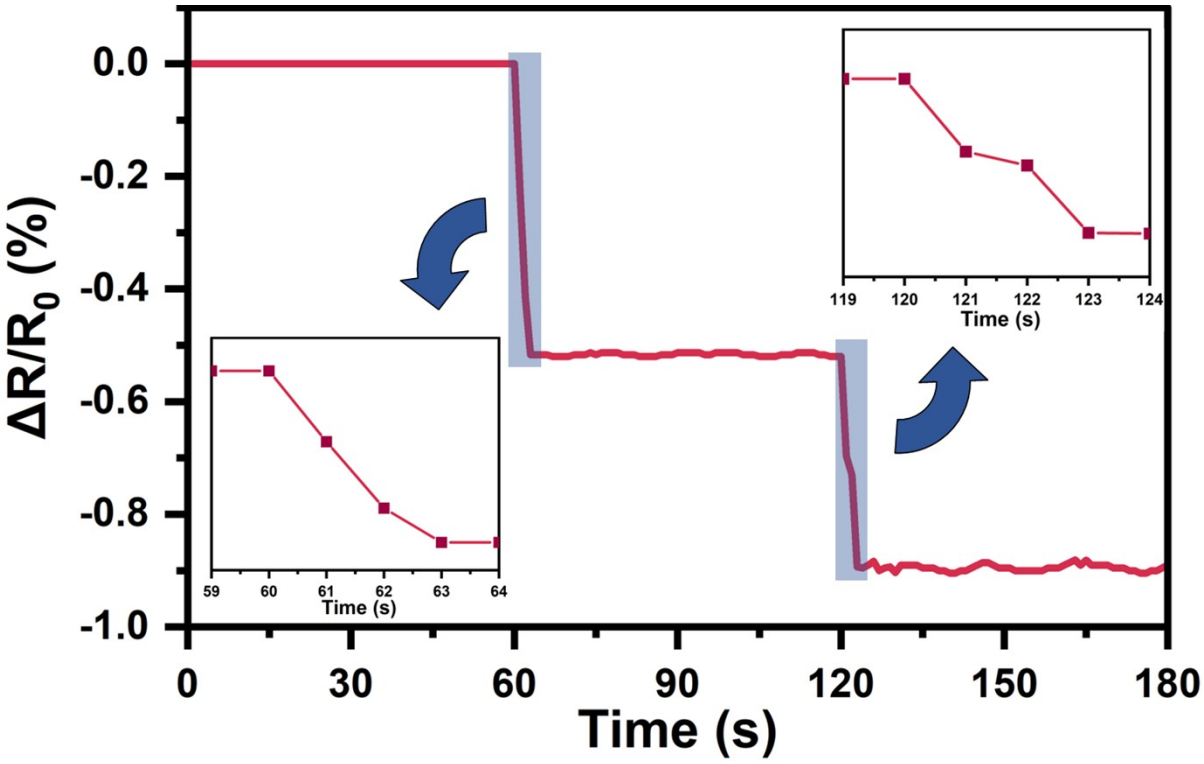

Figure S18. The response time curve of the OEDS patch under quick inject 0.1 μL sweat at the 60th second and the 120th second.

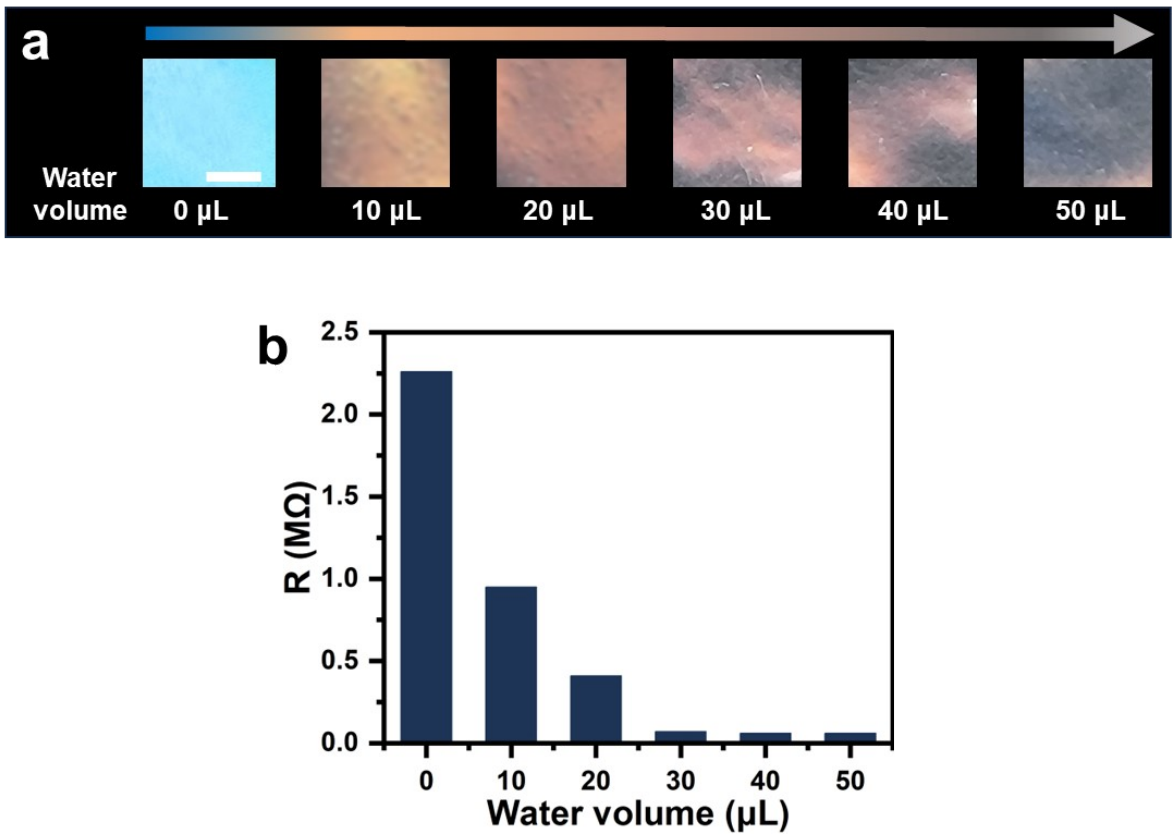

Figure S19. Colorimetric change (a) and relative resistance variations (b) of the CNC/PVA-$PA_{0.7}$ patches in response to varying volumes of water.

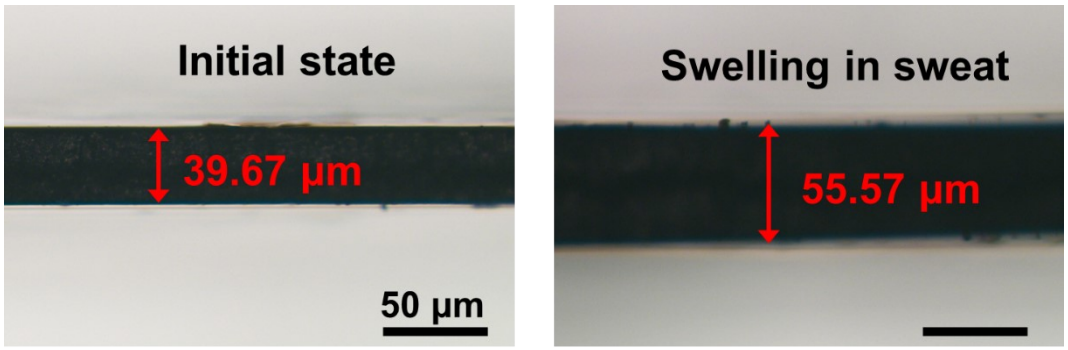

Figure S20. Cross-section images of the OEDS patch before and after swelling in sweat.

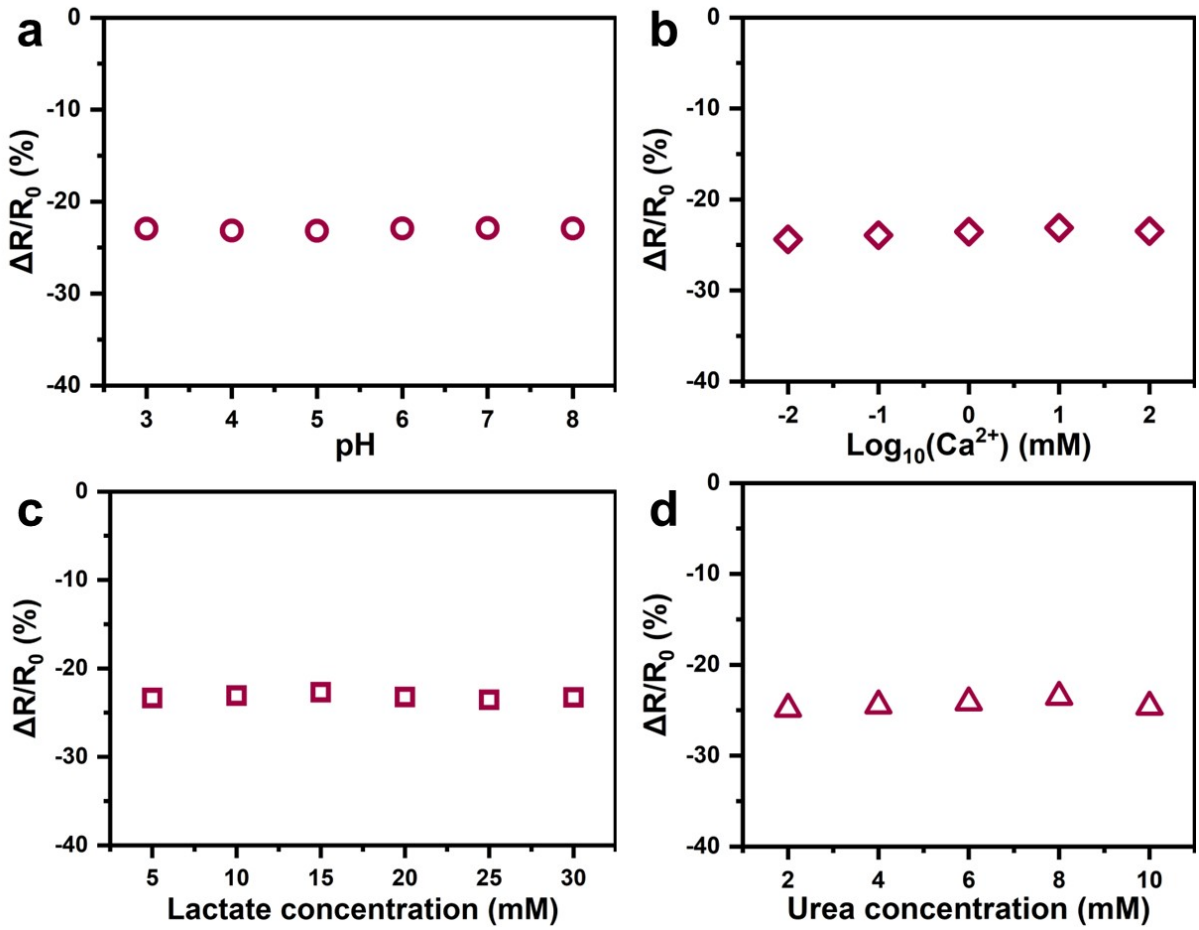

Figure S21. Relationship between resistance change rate ($\Delta R/R_0$) and pH (a), the concentration of Ca^{2+} (b), lactate (c), urea (d) in 10 μL sweat.

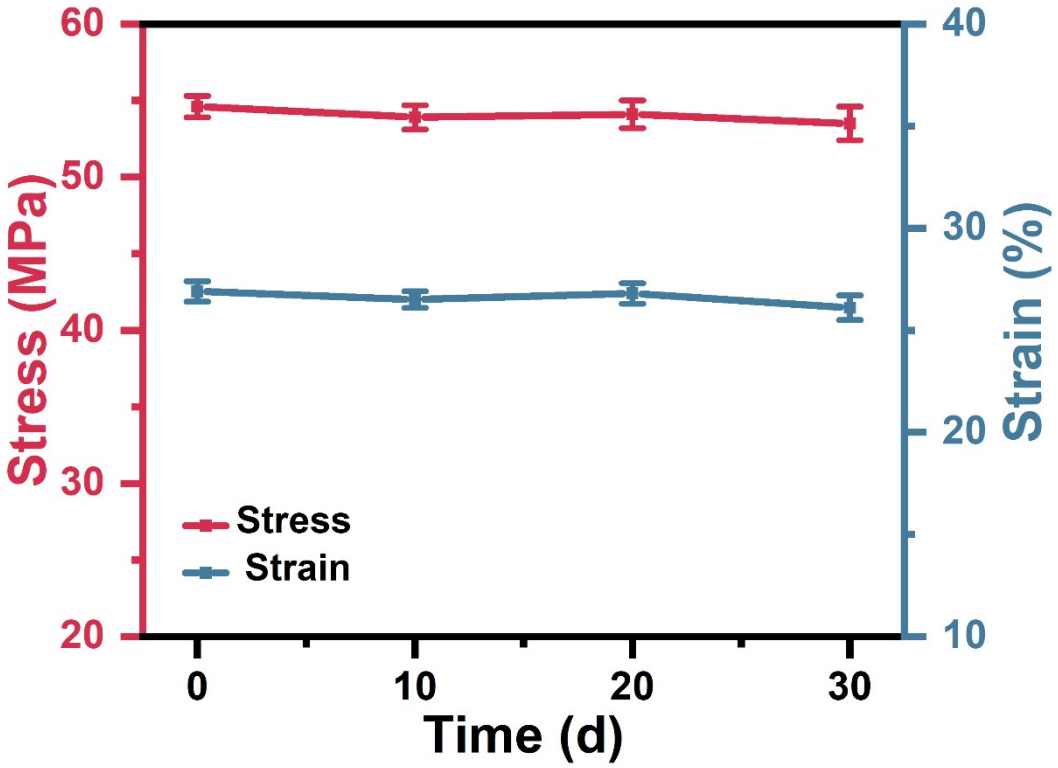

Figure S22. Stress and strain values of patches stored for 0, 10, 20, and 30 days in a dry environment at room temperature.

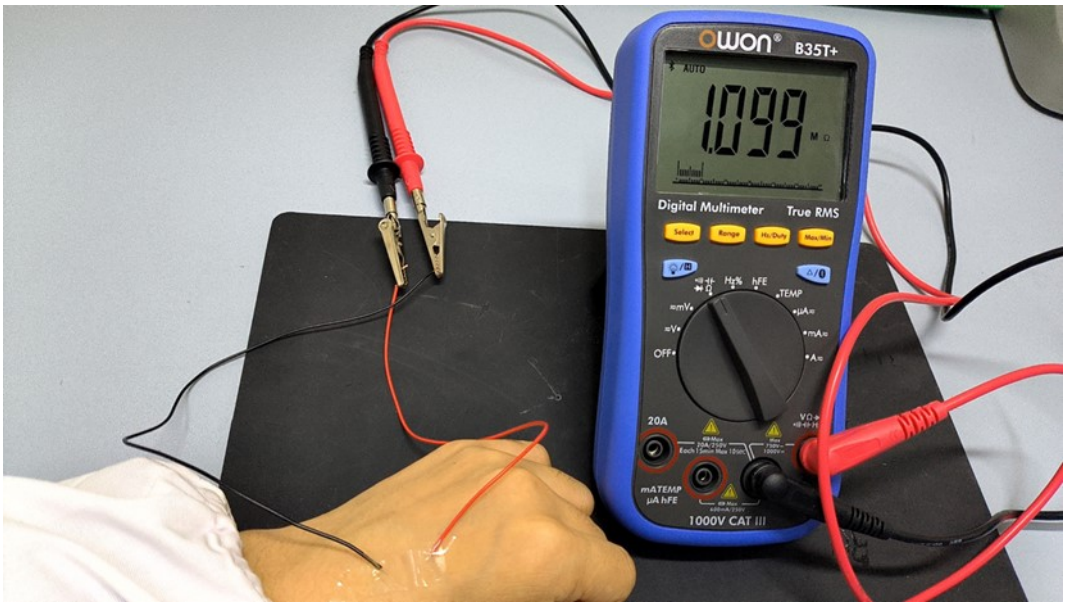

Figure S23. Photograph of the OEDS patch connecting with a multimeter.

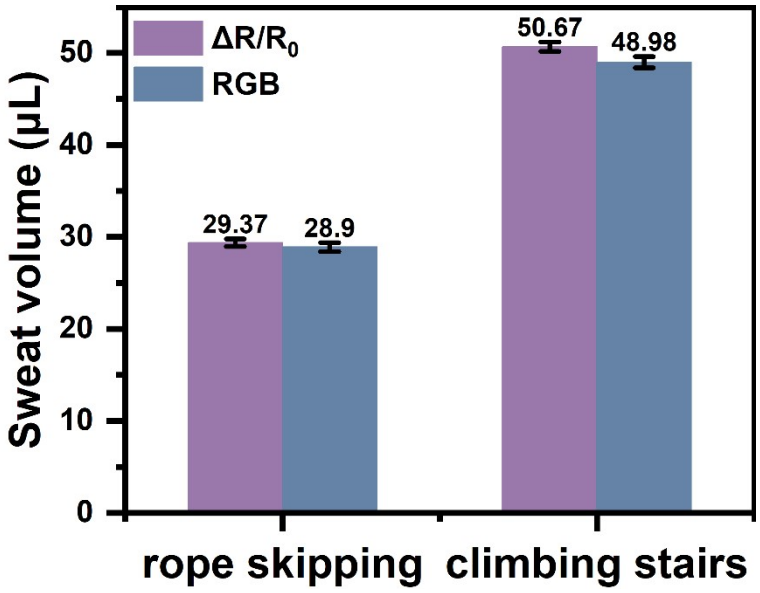

Figure S24. Comparing the calculated sweat volume amount of rope skipping and climbing stairs. from $\Delta R/R_0$ and RGB.

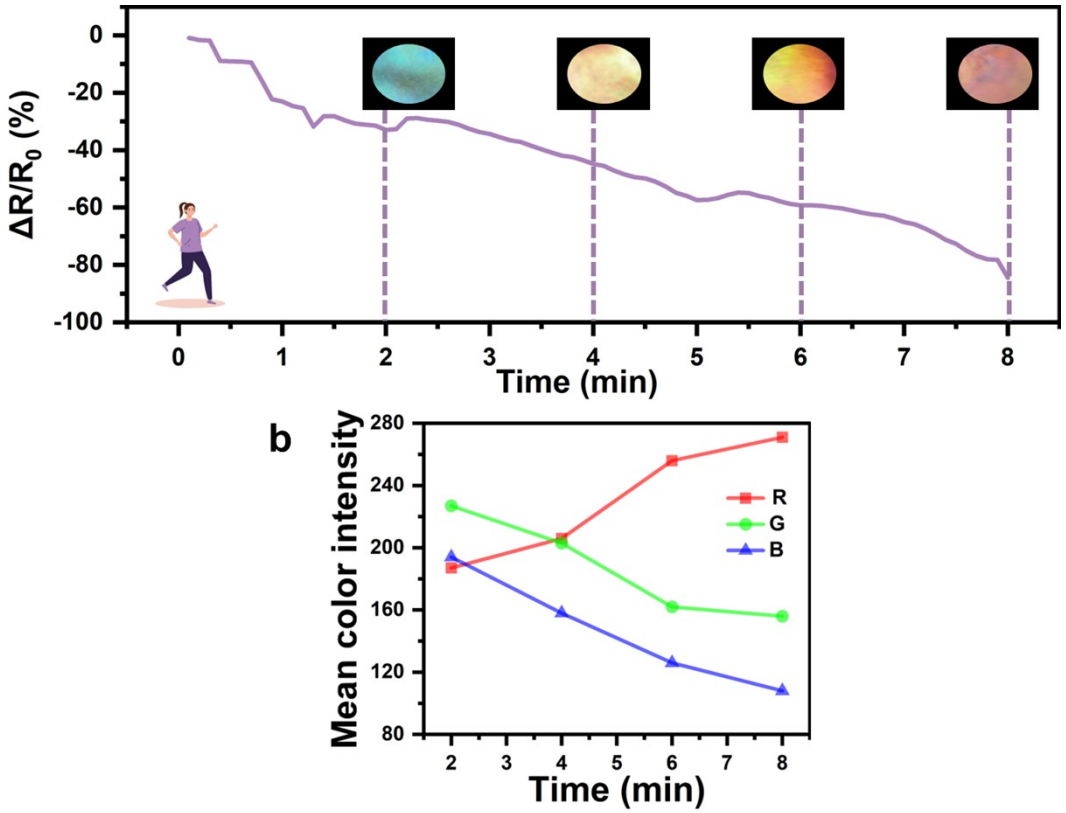

Figure S25. Color and resistivity changes of detection units during running and the corresponding RGB images.

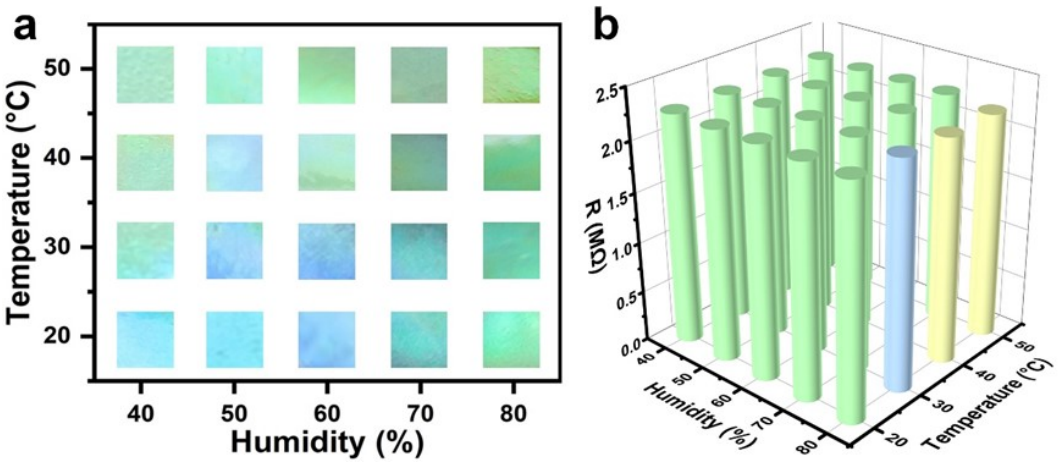

Figure S26. (a) Colorimetric changes observed in the patch under varying humidity and temperature conditions without sweat exposure. (b) Changes in resistance of the patch across different humidity and temperature levels without sweat treatment.

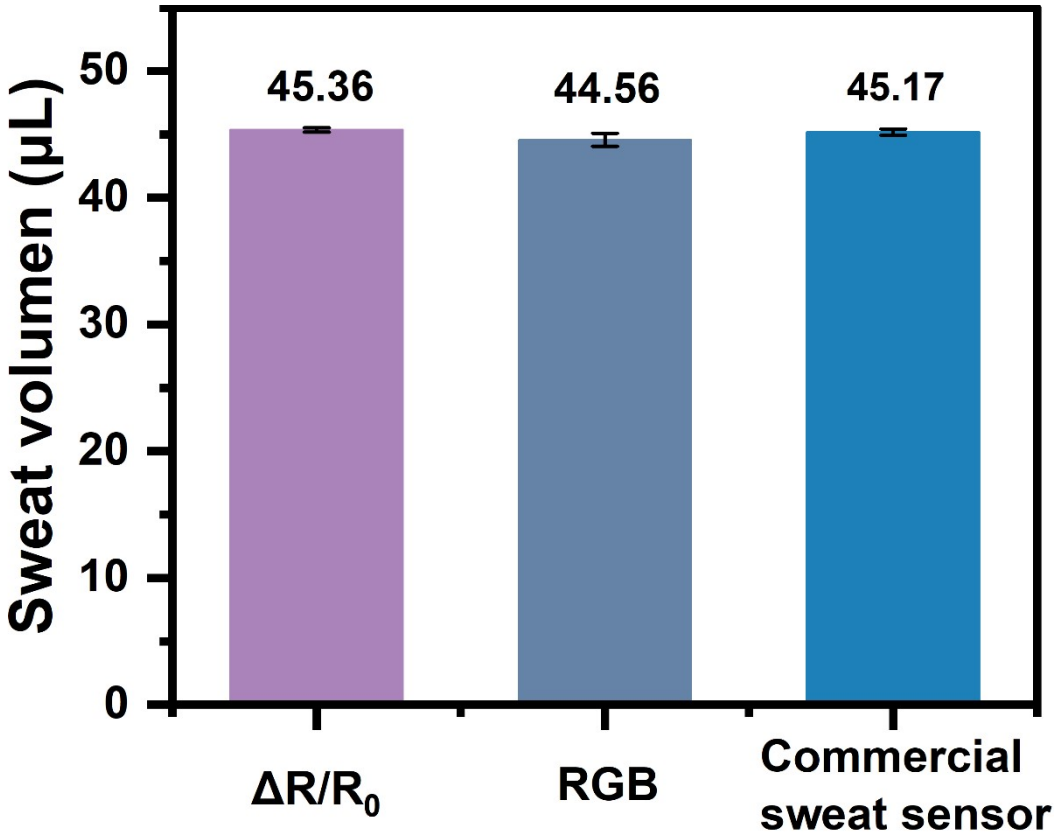

Figure S27. Comparing the volume amount of sweat calculated from $\Delta R/R_0$ and RGB with the measurements from the commercial sweat sensor for 8 minutes of running.

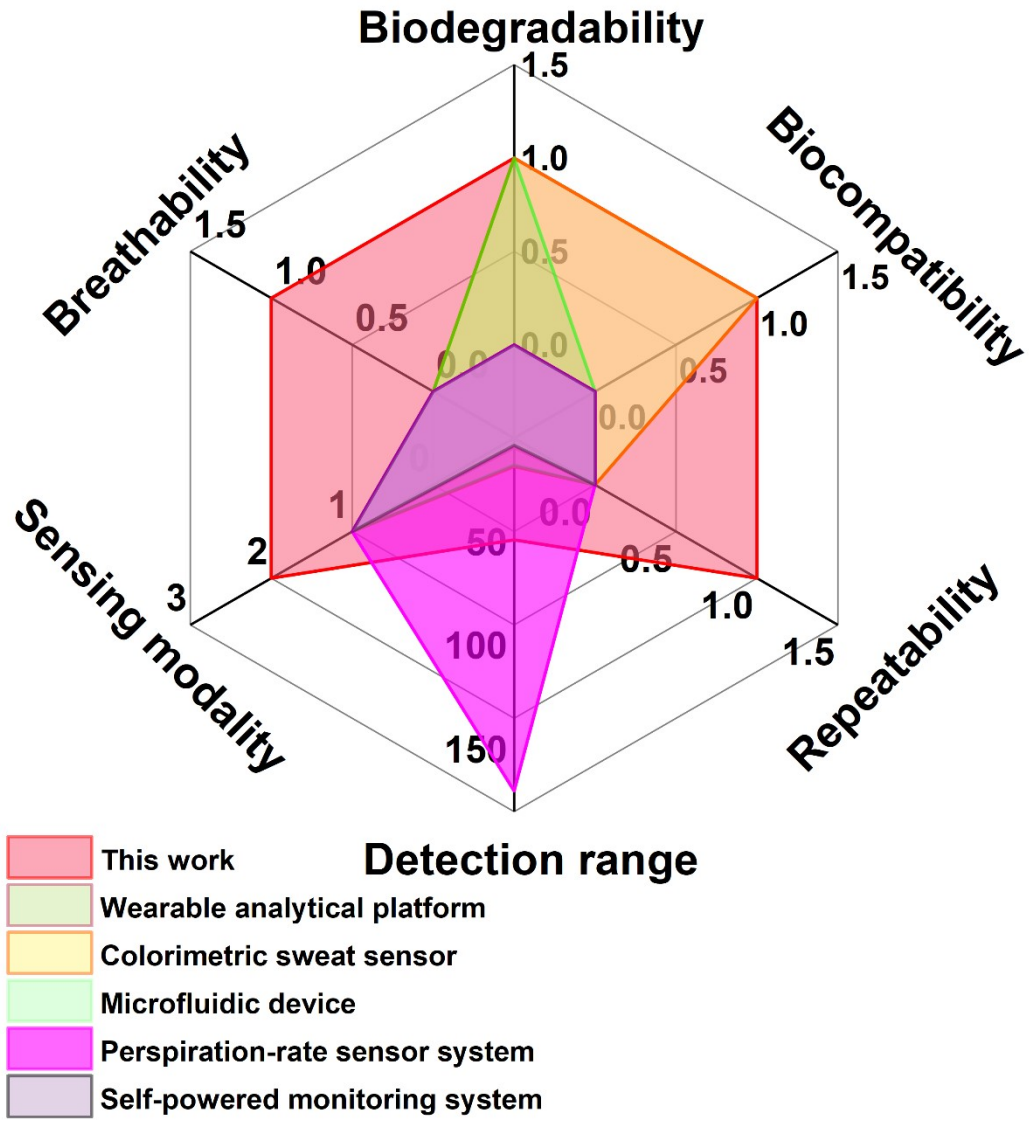

Figure S28. Comprehensive performance comparison with other sweat sensors.[8–12]

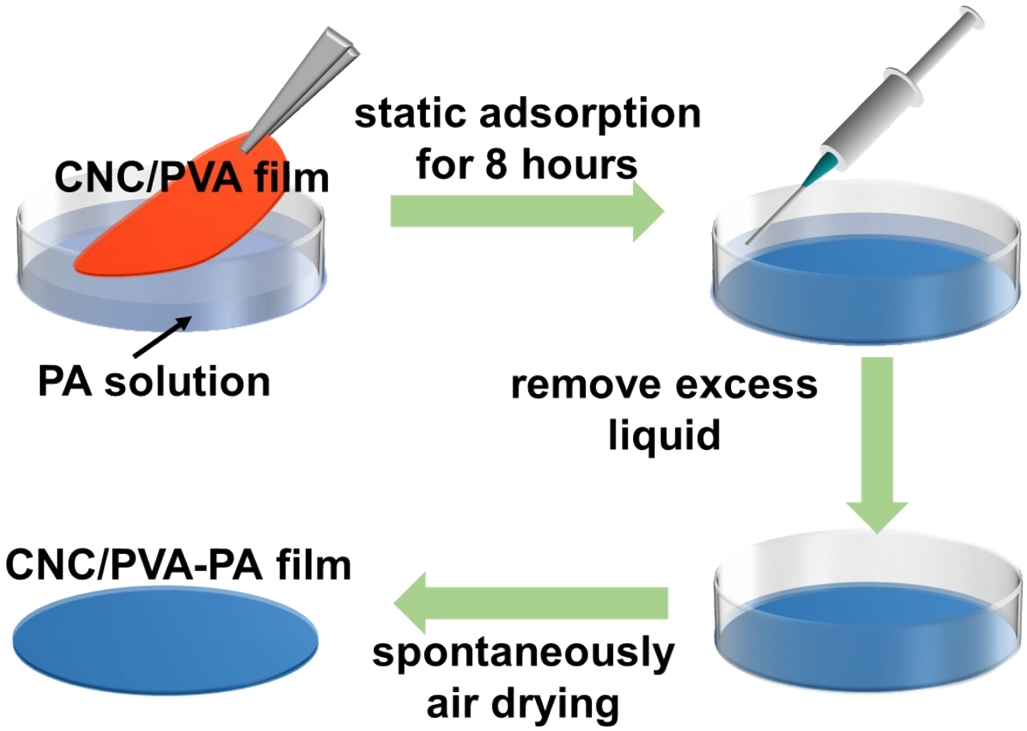

Figure S29. Schematic of the preparation of the CNC/PVA-PA patches

Table S1. Multiplication results of the signs of each cross-peak in 2Dcos synchronous and asynchronous spectra of the CNC/PVA-PA system.

1138	-	+	
1640	-		
3440			
	3440	1640	1138

Table S2. Comparison of stress and toughness values with similar materials reported in the literature.

Name of material	Stress (kPa)	Toughness ($kJ \cdot m^{-3}$)
$CNC/PVA\text{-}PA_{0.7}$	54600	1404
ACTC elastomer[1]	113.5	1160
PVA/CS-PA hydrogel[2]	197	600
PVA−PA hydrogel[3]	1500	637.5
OE-skin[4]	38.8	157.1
PAAm/Cel hydrogel[5]	124.1	990

Table S3. Demonstration form of comprehensive performance for different sweat sensors.

Name of sweat sensor	Sensing modality	Minimum detection limit (μL)	Maximum detection limit (μL)	Repeatability	Breathability	Biodegradability	Biocompatibility
OEDS patches	Optical and electrical dual-signal	1	50	√	√	√	√
Wearable analytical platform[8]	Colorimetric signals and spectrophotometric detection	4	8.5	×	×	×	×
Colorimetric sweat sensor[9]	Colorimetric	2.4	16	×	×	√	√
Microfluidic device[10]	Colorimetric	2	15	×	×	√	×
Perspiration-rate sensor system[11]	Electrochemical impedance	0.6	170	×	×	×	×
Self-powered monitoring system[12]	Voltage and current	2.7	5.9	×	×	×	×

Participation

I agree to participate in this research by wearing the OEDS patch to collect sweat and further detect sports activities.

15th, March,2024

References

1 X. Zhang, Q. Fu, Y. Wang, H. Zhao, S. Hao, C. Ma, F. Xu and J. Yang, *Adv. Funct. Mater.*, 2024, **34**, 2307400.

2 L. Zeng, B. Liu and G. Gao, *Sci. China Mater.*, 2023, **66**, 4062–4070.

3 S. Zhang, Y. Zhang, B. Li, P. Zhang, L. Kan, G. Wang, H. Wei, X. Zhang and N. Ma, *ACS Appl. Mater. Interfaces*, 2019, **11**, 32441–32448.

4 H. Zhang, H. Chen, J.-H. Lee, E. Kim, K.-Y. Chan, H. Venkatesan, X. Shen, J. Yang and J.-K. Kim, *ACS Nano*, 2023, **17**, 5921–5934.

5 S. Wang, Z. Wang, L. Zhang, Z. Song, H. Liu and X. Xu, *Chem. Eng. J.*, 2024, **492**, 152290.

6 Z. Ma, Q. Huang, Q. Xu, Q. Zhuang, X. Zhao, Y. Yang, H. Qiu, Z. Yang, C. Wang, Y. Chai and Z. Zheng, *Nat. Mater.*, 2021, **20**, 859–868.

7 Z. Sonner, E. Wilder, J. Heikenfeld, G. Kasting, F. Beyette, D. Swaile, F. Sherman, J. Joyce, J. Hagen, N. Kelley-Loughnane and R. Naik, *Biomicrofluidics*, 2015, **9**, 031301.

8 A. Vaquer, E. Barón and R. De La Rica, *ACS Sens.*, 2021, **6**, 130–136.

9 X. Yue, F. Xu, L. Zhang, G. Ren, H. Sheng, J. Wang, K. Wang, L. Yu, J. Wang, G. Li, G. Lu and H.-D. Yu, *ACS Sens.*, 2022, **7**, 2198–2208.

10 S. Liu, D. S. Yang, S. Wang, H. Luan, Y. Sekine, J. B. Model, A. J. Aranyosi, R. Ghaffari and J. A. Rogers, *EcoMat*, 2023, **5**, e12270.

11 S. Honda, R. Tanaka, G. Matsumura, N. Seimiya and K. Takei, *Adv. Funct. Mater.*, 2023, **33**, 2306516.

12 G. Xu, X. Huang, R. Shi, Y. Yang, P. Wu, J. Zhou, X. He, J. Li, Y. Zen, Y. Jiao, B. Zhang, J. Li, G. Zhao, Y. Liu, Y. Huang, M. Wu, Q. Zhang, Z. Yang and X. Yu, *Adv. Funct. Mater.*, 2023, **34**, 2310777.